

Electronic Supplementary Information:

Temperature-dependent hysteresis effects on perovskite-based solar cells

Luis K. Ono, Sonia R. Raga, Shenghao Wang, Yuichi Kato, Yabing Qi*

Energy Materials and Surface Sciences Unit (EMSS), Okinawa Institute of Science and Technology Graduate University (OIST), 1919-1 Tancha, Onna-son, Okinawa 904-0495 Japan.

*E-mail: Yabing.Qi@oist.jp

Contents:

1. Experimental section. (Page 3–5)
2. PCE under AM1.5G. (Page 6)
3. Circuit diagram showing the electric connections in the probe-station. (Page 7)
4. Time-dependent photocurrent and dark current responses as a function of applied stair-step function. (Pages 8–10)
5. Semi-logarithmic plots of photocurrent responses. (Page 11–16)
6. I_{sc} , V_{oc} , and FF as a function of perovskite solar cell temperature. (Page 17)
7. Tabulated time-constants corresponding to the slowest process (τ_{slow}). (Page 18)

8. Tabulated I_{sc} , V_{oc} , and FF as a function of the delay time (t_d) in forward and reverse and with the sample held at three different temperatures (250 K, 300 K, 360 K). (Page 19–20)
9. References (21–22)

Experimental section:

Methylammonium iodide synthesis. MAI was synthesized according to a literature procedure with slight modification [1]. Briefly, hydroiodic acid solution was gradually added to methyl amine ethanol solution that was kept stirring in an ice-bath. Ethanol and water from the mixed solution was evaporated using a rotary evaporator (BUCHI, Rotavapor R-3). The precipitated yellow-colored crystals were dissolved in hot ethanol, and cooled in a refrigerator at 5 °C for recrystallization. Subsequently, the crystals were filtered and washed with tetrahydrofuran resulting in white crystal powder. We dried and kept the MAI in N₂ glove box (<0.1 ppm of O₂ and H₂O).

Perovskite film deposition. Perovskite films were deposited on fluorine doped tin oxide (FTO) glass pre-coated with a compact layer of TiO₂ (c-TiO₂) as reported elsewhere [2, 3]. The solution processed perovskite film was prepared using the following procedure: MAI and PbCl₂ (Sigma-Aldrich) were dissolved in *N,N*-dimethylformamide with molar concentrations of 2.64 M and 0.88 M, respectively. The precursor solution was left stirring overnight to completely dissolve. 50 μL of perovskite precursor was spin-coated on the c-TiO₂/FTO at 2000 rpm for 30 seconds followed by a thermal annealing at 110°C for 45min. Only the last step of the thermal annealing was conducted in the laboratory ambient air (inside cleanroom class 100). All other solution and sample preparation steps were conducted inside the N₂ glove box.

Perovskite film characterization and solar cell fabrication. The substrates with the as-grown perovskite films were immediately transferred to the N₂ glove box for the complete device fabrication. The properties of the perovskite films were studied by x-ray diffraction (XRD, D8 Bruker) and scanning electron microscope (SEM, FEI Quanta 250 FEG). The solar cell device fabrication was completed by spin-coating a hole transport layer (HTM) that consists of a mixture of three materials: spiro-MeOTAD (2,2',7,7'-tetrakis(*N,N*-di-p-methoxy-phenylamine)-9,9'-spirobifluorene (Merck) dissolved in chlorobenzene (72.5 mg/mL), 17.5 μL of Li-bis(trifluoromethanesulfonyl)-imide (LiTFSI, Sigma) dissolved in acetonitrile (52 mg/100 μL), and 28.8 μL of tert-butylpyridine (*t*-BP, Sigma) [2, 3]. Finally, the Au top electrodes (100 nm) were deposited by thermal evaporation through a shadow mask defining solar cell active areas of ~0.09 cm². Current-voltage device characteristics were measured by applying an external potential bias under standard 1 sun AM1.5G

simulated solar irradiation (100 mW/cm^2 , Newport Oriel Sol1A) and measuring the photocurrent generated (Keithley 2420 source meter). Current-voltage characteristics of a reference Si solar cell measured under standard AM1.5G test conditions (black curve) and the same Si cell under the microscope light exposure used in the probe-station (red curve) to illuminate the samples. Based on the short-circuit current (I_{sc}) comparisons roughly the microscope light intensity was observed to correspond to ~9% of AM1.5G.

Capacitance (admittance) measurements on various types of solar cells. Hysteresis characterization studies performed with staircase voltage is not available on CIGS and CdS/CdTe solar cells because usually capacitance values are small for these cells (below $\mu\text{F/cm}^2$) [4-10]. The staircase voltage I-V measurements on Si cell (on the order of $\mu\text{F/cm}^2$) [11-13], which shows an immediate photocurrent response without the transient behavior, have been reported by Kim and Park, which is provided as a comparison to the perovskite cell [11]. OPV devices have the complexity due to the large number of organic semiconductors used for fabricating OPV devices. Based on our literature study, for the specific cases of the commonly employed cell structures such as ITO/PEDOT/P3HT:PCBM/Al [14-16], ITO/PEDOT/PBTPD:PCBM/Al [17], ITO/CuPc/C60/BCP/Al [18], ITO/MeO-TPD/ZnPc:C60/C60/Al [19], capacitance values were reported to be on the order of nF/cm^2 . Thus, no hysteresis effects were reported on the above mentioned OPVs. Dye sensitized solar cells (DSSCs) capacitance is in the order of mF/cm^2 [20]. Tian et al. reported on the first transient measurements by applying the staircase voltage function on DSSCs [12].

Procedure for the extraction of steady-state I-V curve. This section provides a step by step procedure to illustrate the extraction of steady-state I-V curves (the one similar to Fig. 5) on the basis of the staircase voltage sweep measurements (Figs. 2 and S3-S5).

Step 1. Each voltage step with 8 s time interval is analyzed fitting multi-exponential function as shown in Equations (1) and (2) in the main text.

Step 2. For the data displayed in Fig. 1, minimum of three terms ($i=0,1,2$) were needed to reproduce the raw data giving reasonably low χ^2 . The number of exponential terms needed to fit the rawdata with low χ^2 may vary depending on the sample preparation conditions.

Step 3. Based on the fittings above, the extrapolated steady-state photocurrents $I(\infty)$ are extracted and steady-state I-V curves generated.

Step 4. The determination of time constants were conducted plotting $\ln\left[\frac{I(t_0) - I(\infty)}{I(t) - I(\infty)}\right]$

(forward scan) and $\ln\left[\frac{I(t) - I(\infty)}{I(t_0)}\right]$ (reverse scan) versus time plots.

Step 5. A linear regime was fitted using least-square fitting method and time constants determined from the linearly fitted slopes.

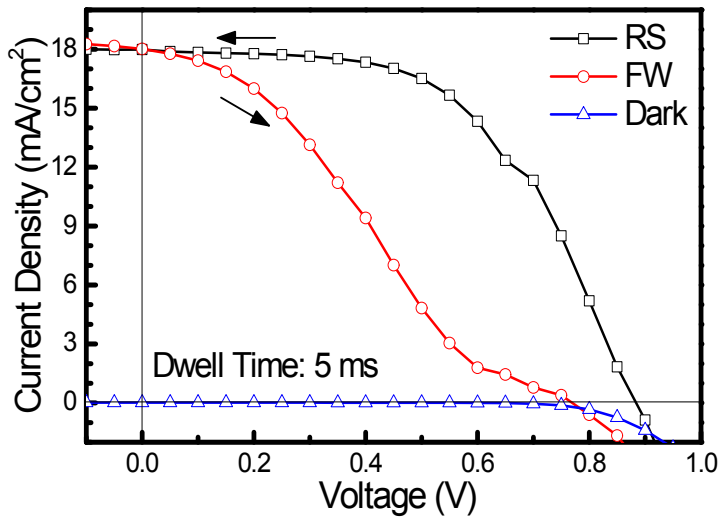


Figure S1. J-V curves under 1 sun (AM1.5G). These J-V curves have an average sweep rate of 0.45 V/s with 5 ms dwell time and 30 measured points.

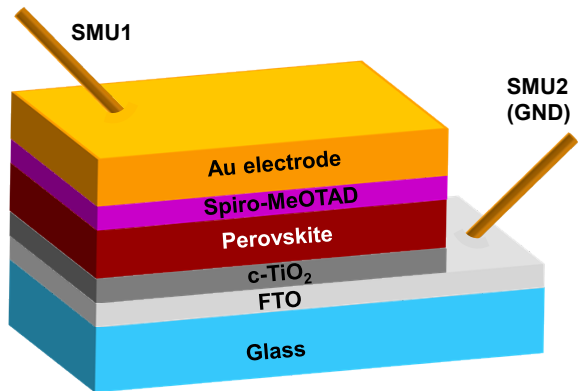


Figure S2. Circuit diagram showing the electric connections in the probe station. The Source Measure Units (SMUs) are connected in such the FTO is grounded (GND) and BIAS applied to the top Au electrode.

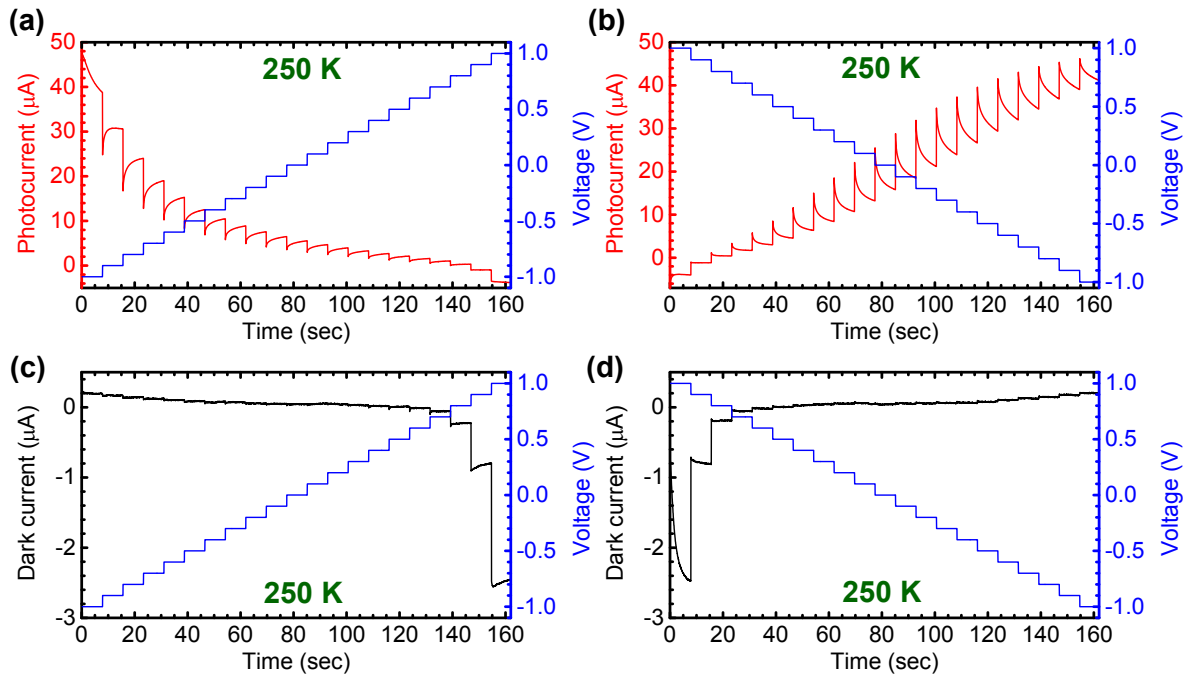


Figure S3. Photocurrent and dark current as a function of applied voltage that varies as a staircase function. The voltage sweep from zero to positive voltage and from positive to zero are denoted as forward scan (a, c) and reverse scan (b, d), respectively. The step delayed photocurrent responses of ~ 8 s long are shown when the sample is held at 250 K. The sharp jumps observed in the current signals after the each step-voltage are indicative of the capacitive effects in the device.

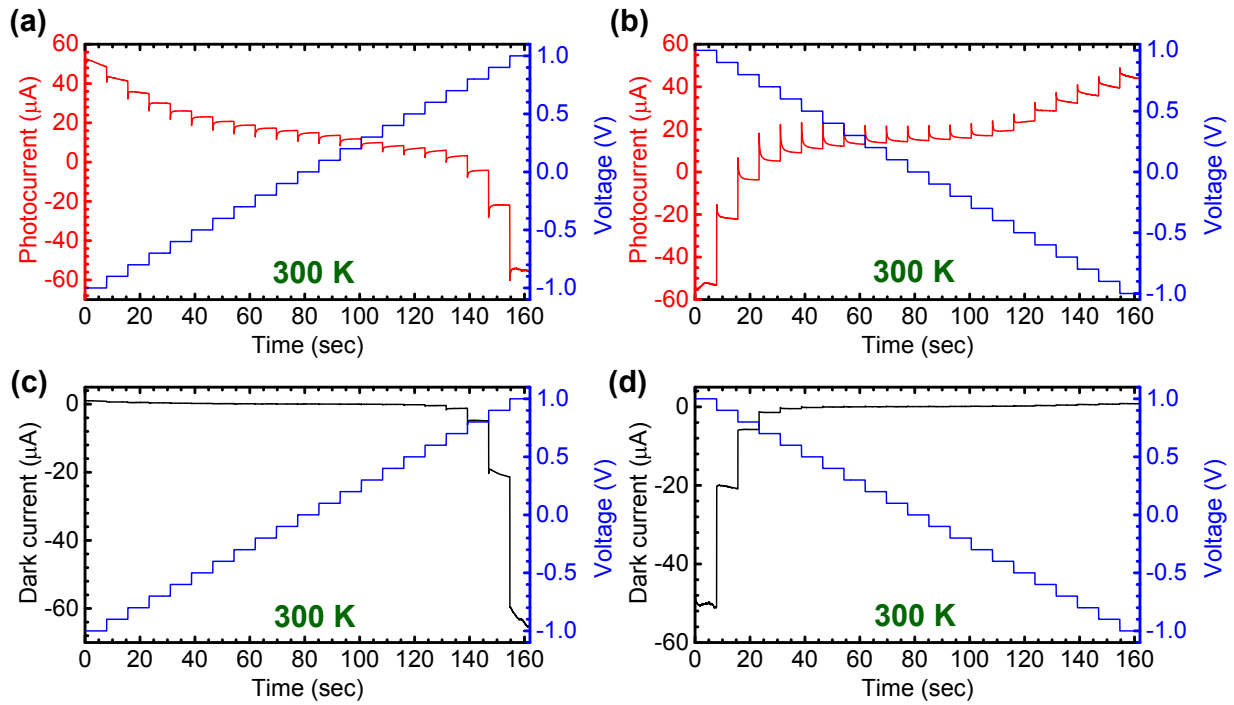


Figure S4. Photocurrent and dark current as a function of applied voltage that varies as a staircase function. The voltage sweep from zero to positive voltage and from positive to zero are denoted as forward scan (a, c) and reverse scan (b, d), respectively. The step delayed photocurrent responses of ~ 8 s long are shown when the sample is held at 300 K.

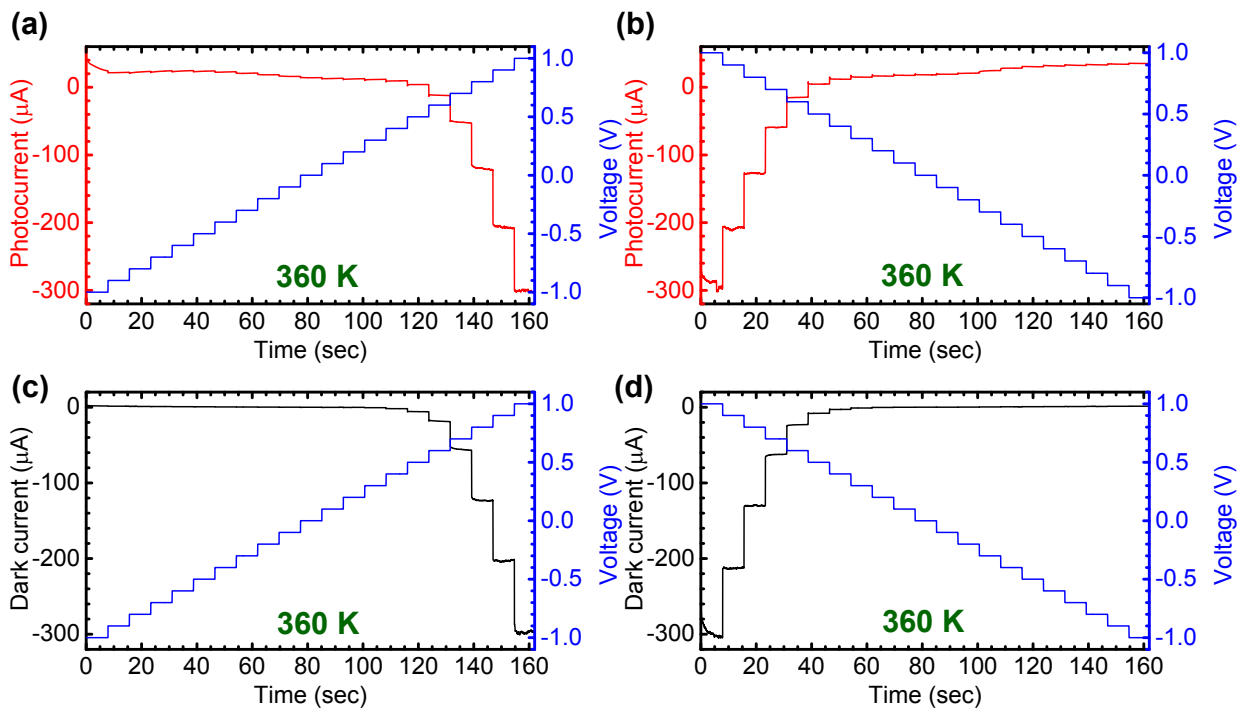


Figure S5. Photocurrent and dark current as a function of applied voltage that varies as a staircase function. The voltage sweep from zero to positive voltage and from positive to zero are denoted as forward scan (a, c) and reverse scan (b, d), respectively. The step delayed photocurrent responses of ~ 8 s long are shown when the sample is held at 360 K.

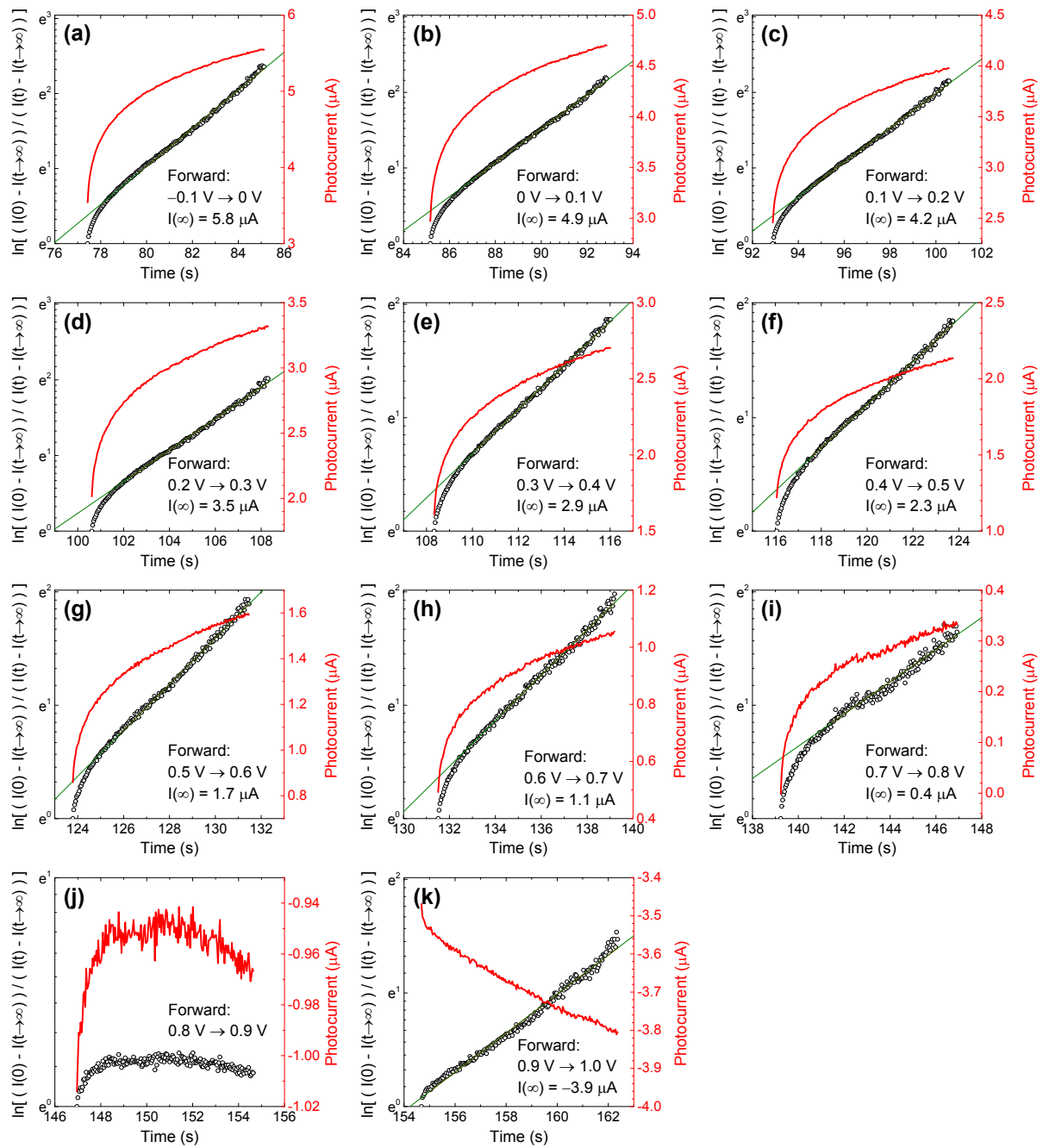


Figure S6. Semi-logarithmic plot of the photocurrent responses as a function of applied voltage step in the forward scan direction when perovskite solar cell is under illumination at 250 K. The spectra show that multiple processes, characterized by τ_{fast} and τ_{slow} , take place for the charge transport within the perovskite based solar cell.

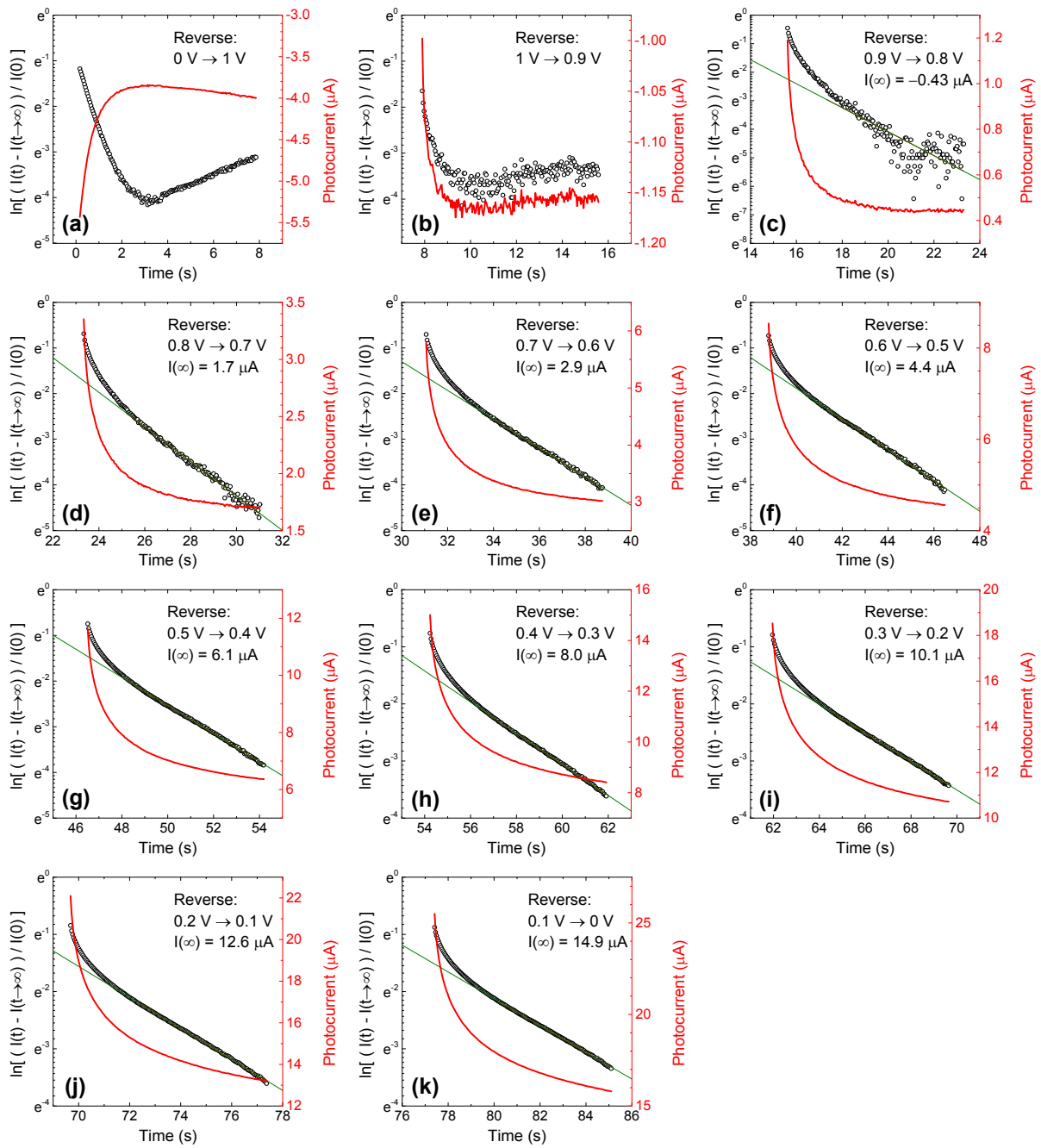


Figure S7. Semi-logarithmic plot of the photocurrent responses as a function of applied voltage step in the reverse scan direction when perovskite solar cell is under illumination at 250 K.

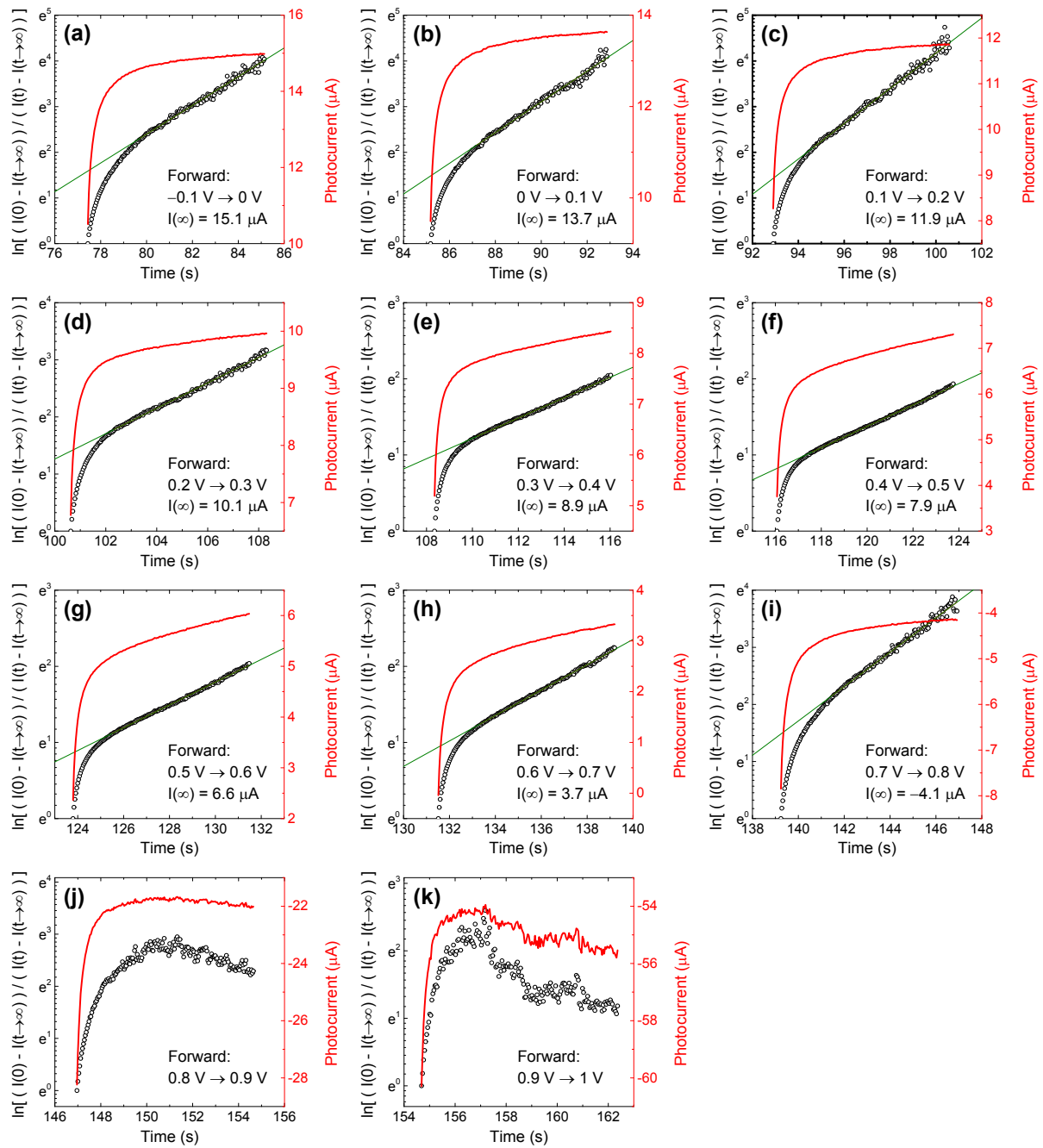


Figure S8. Semi-logarithmic plot of the photocurrent responses as a function of applied voltage step in the forward scan direction when perovskite solar cell is under illumination at 300 K.

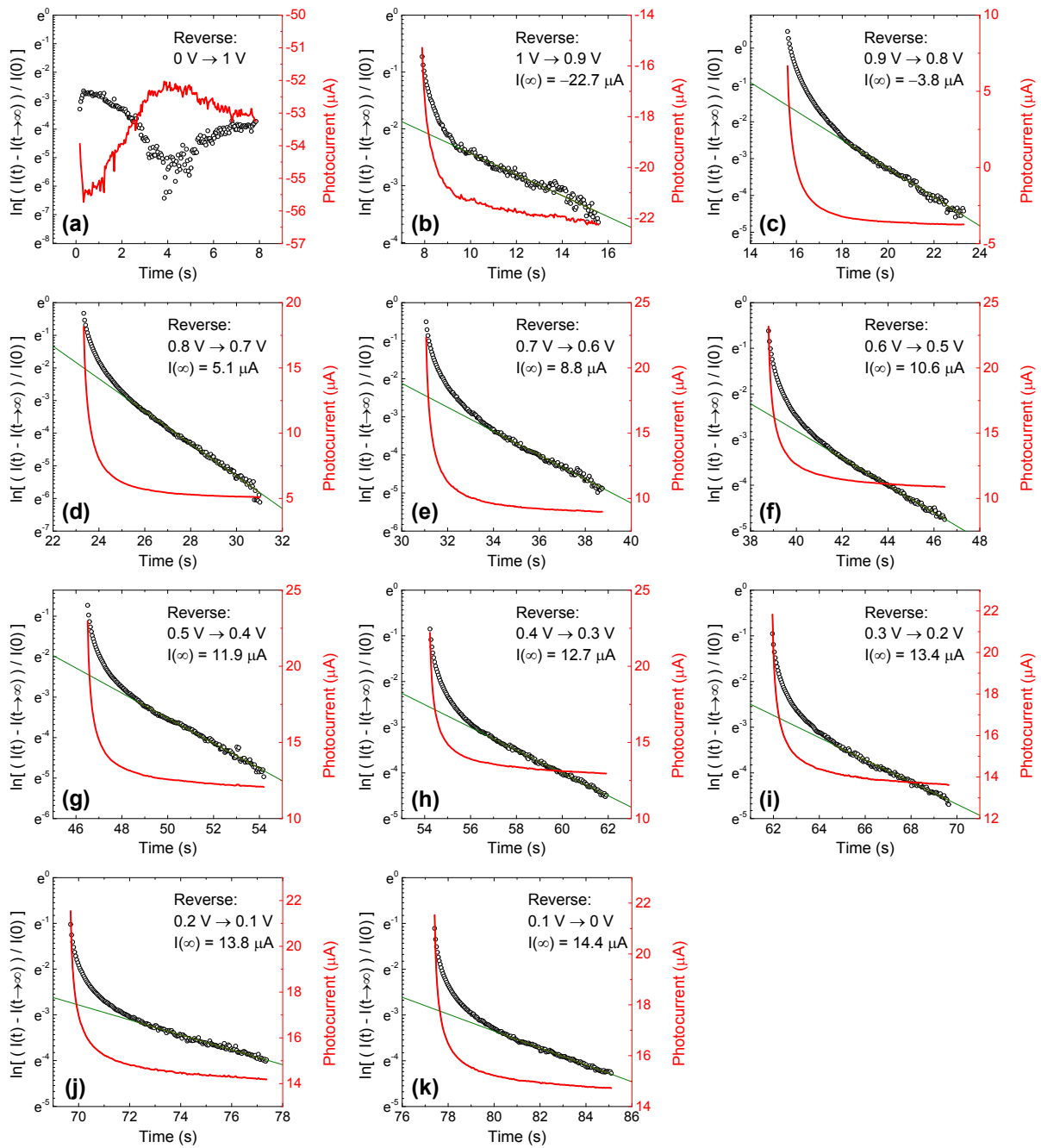


Figure S9. Semi-logarithmic plot of the photocurrent responses as a function of applied voltage step in the reverse scan direction when perovskite solar cell is under illumination at 300 K.

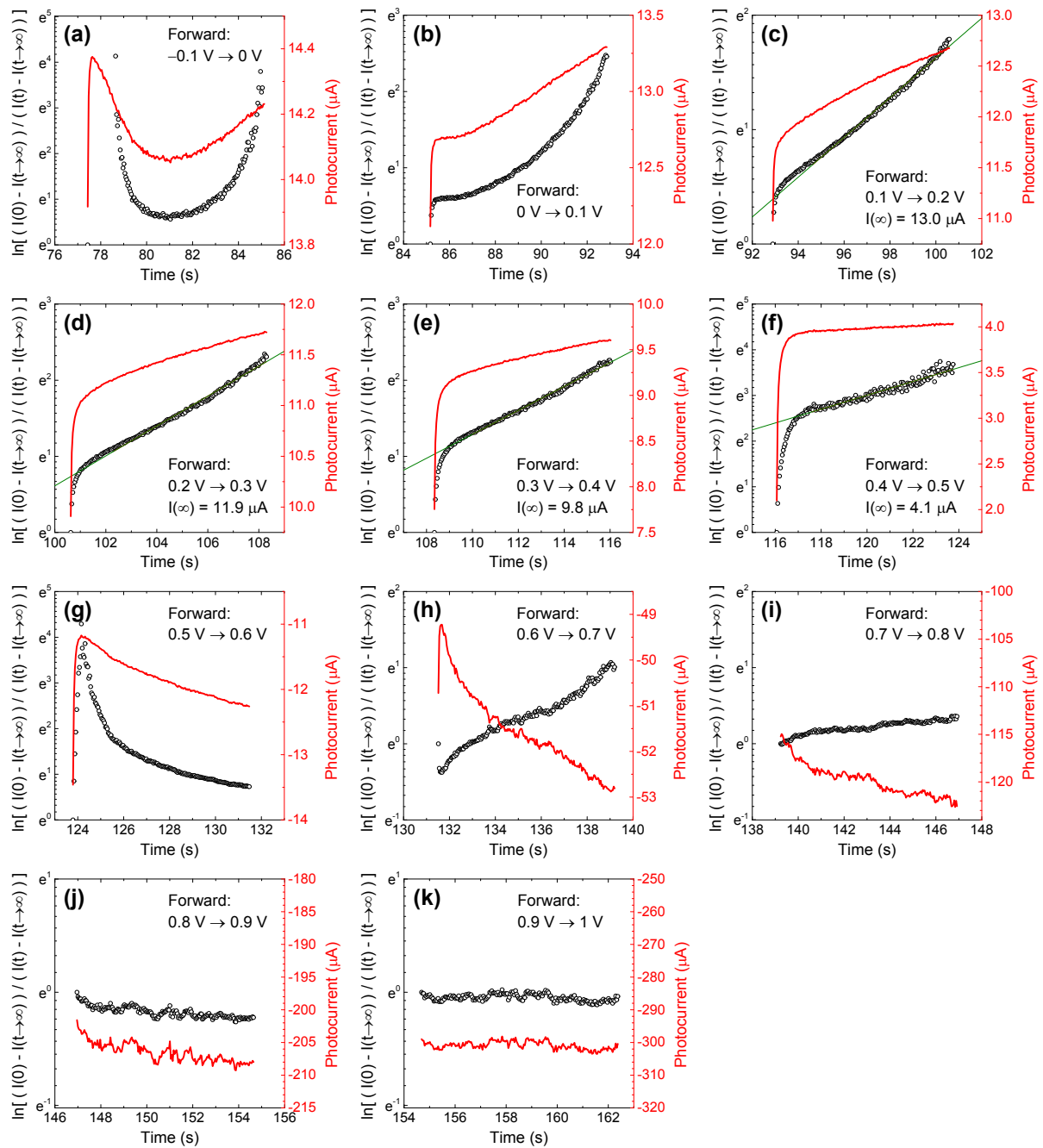


Figure S10. Semi-logarithmic plot of the photocurrent responses as a function of applied voltage step in the forward scan direction when perovskite solar cell is under illumination at 360 K

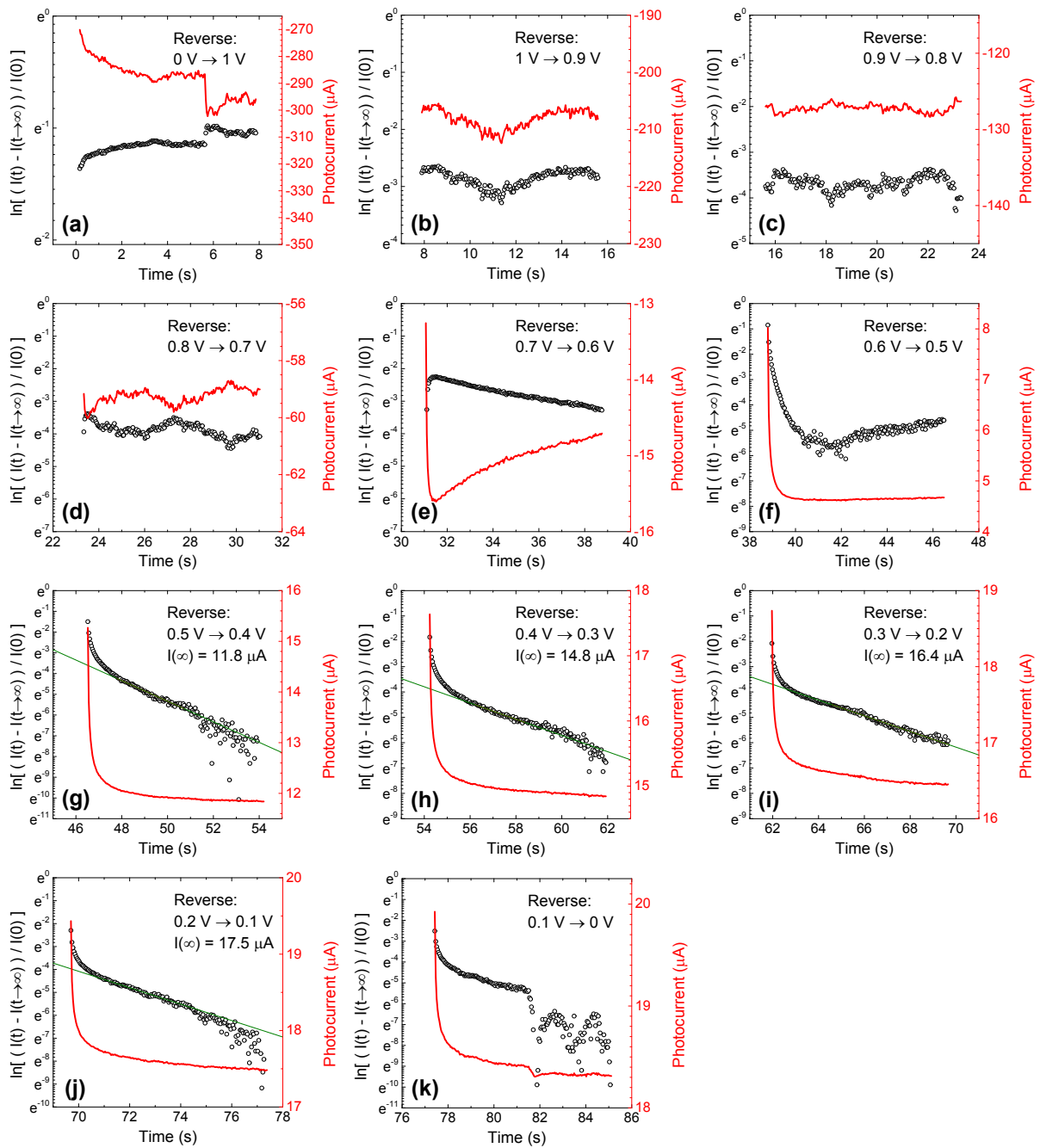


Figure S11. Semi-logarithmic plot of the photocurrent responses as a function of applied voltage step in the reverse scan direction when perovskite solar cell is under illumination at 360 K.

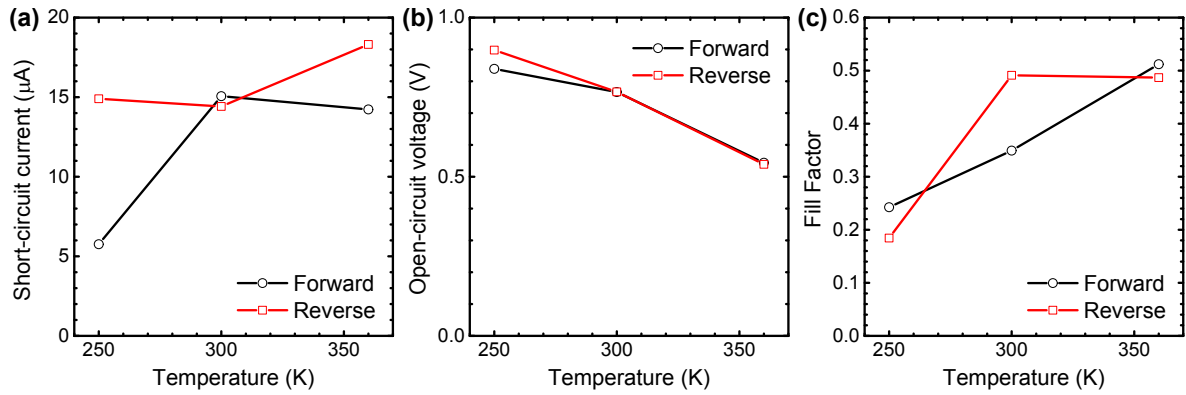


Figure S12. Extracted (a) short-circuit current, (b) open-circuit voltage, and fill factor parameters as a function of temperature with the I-V curves corresponding to the steady-state conditions ($t_d \rightarrow \infty$, Figure 4).

250 K			
Forward		Reverse	
Voltage (V)	τ_{slow} (s)	Voltage (V)	τ_{slow} (s)
-0.1 → 0	3.94 ± 0.02	0.9 → 0.8	2.38 ± 0.12
0 → 0.1	4.46 ± 0.02	0.8 → 0.7	2.64 ± 0.02
0.1 → 0.2	4.40 ± 0.02	0.7 → 0.6	3.18 ± 0.01
0.2 → 0.3	4.80 ± 0.02	0.6 → 0.5	2.97 ± 0.01
0.3 → 0.4	5.15 ± 0.02	0.5 → 0.4	3.25 ± 0.01
0.4 → 0.5	5.27 ± 0.02	0.4 → 0.3	3.67 ± 0.01
0.5 → 0.6	4.92 ± 0.03	0.3 → 0.2	4.01 ± 0.01
0.6 → 0.7	4.98 ± 0.05	0.2 → 0.1	3.69 ± 0.01
0.7 → 0.8	7.05 ± 0.12	0.1 → 0	4.27 ± 0.01
300 K			
Forward		Reverse	
Voltage (V)	τ_{slow} (s)	Voltage (V)	τ_{slow} (s)
-0.1 → 0	3.17 ± 0.03	0.9 → 0.8	2.57 ± 0.02
0 → 0.1	2.97 ± 0.03	0.8 → 0.7	2.01 ± 0.02
0.1 → 0.2	2.59 ± 0.02	0.7 → 0.6	3.18 ± 0.03
0.2 → 0.3	4.50 ± 0.03	0.6 → 0.5	3.35 ± 0.02
0.3 → 0.4	7.49 ± 0.03	0.5 → 0.4	3.23 ± 0.03
0.4 → 0.5	7.12 ± 0.02	0.4 → 0.3	4.01 ± 0.02
0.5 → 0.6	6.69 ± 0.02	0.3 → 0.2	4.11 ± 0.03
0.6 → 0.7	5.99 ± 0.02	0.2 → 0.1	6.12 ± 0.07
0.7 → 0.8	3.32 ± 0.03	0.1 → 0	5.41 ± 0.04
360 K			
Forward		Reverse	
Voltage (V)	τ_{slow} (s)	Voltage (V)	τ_{slow} (s)
0.1 → 0.2	4.95 ± 0.07	0.4 → 0.3	2.01 ± 0.04
0.2 → 0.3	4.11 ± 0.07	0.3 → 0.2	3.12 ± 0.10
0.3 → 0.4	5.55 ± 0.15	0.2 → 0.1	3.23 ± 0.05
0.4 → 0.5	4.94 ± 0.30	0.1 → 0	2.79 ± 0.07

Table S1. Extracted time-constants corresponding to the slowest process (τ_{slow}) observed in the semi-logarithmic plot of the transient part of the photocurrent response upon applied voltage.

Temperature / voltage scan direction	t_d	I_{sc} (μA)	V_{oc} (V)	FF
250 K Forward	0	3.5	0.80	0.23
	40 ms	3.7	0.81	0.23
	200 ms	4.1	0.81	0.23
	1 s	4.5	0.82	0.23
	∞	5.8	0.84	0.24
250 K Reverse	0	25.5	0.91	0.20
	40 ms	24.6	0.90	0.20
	200 ms	22.9	0.90	0.20
	1 s	20.3	0.90	0.19
	∞	14.9	0.90	0.18
Temperature / voltage scan direction	t_d	I_{sc} (μA)	V_{oc} (V)	FF
300 K Forward	0	10.5	0.71	0.28
	40 ms	11.3	0.72	0.28
	200 ms	12.6	0.74	0.29
	1 s	14	0.75	0.29
	∞	15.1	0.77	0.35
300 K Reverse	0	21.5	0.84	0.76*
	40 ms	20.0	0.83	0.72*
	200 ms	17.9	0.81	0.64
	1 s	16.1	0.79	0.55
	∞	14.4	0.77	0.49
Temperature / voltage scan direction	t_d	I_{sc} (μA)	V_{oc} (V)	FF
360 K Forward	0	13.9	0.53	0.44
	40 ms	14.3	0.54	0.45
	200 ms	14.4	0.54	0.46
	1 s	14.3	0.54	0.48
	∞	14.2	0.54	0.51
360 K Reverse	0	19.9	0.55	0.55
	40 ms	19.3	0.55	0.53
	200 ms	18.8	0.54	0.51
	1 s	18.6	0.54	0.50
	∞	18.3	0.54	0.49

Table S2. Photovoltaic parameters of short-circuit current (I_{sc}), open-circuit voltage (V_{oc}), and fill factor (FF) calculated from Figure 4 (main text) as a function of the delay time (t_d) in forward and reverse voltage scan directions and with the sample held at three different temperatures (250 K, 300 K, 360 K). The FFs followed by an * show high values caused by the fast voltage sweep (i.e., shorter t_d).

References:

- [1] M.M. Lee, J. Teuscher, T. Miyasaka, T.N. Murakami, and H.J. Snaith, *Efficient Hybrid Solar Cells Based on Meso-Superstructured Organometal Halide Perovskites*. Science **338** (2012) 643-647.
- [2] M.Z. Liu, M.B. Johnston, and H.J. Snaith, *Efficient planar heterojunction perovskite solar cells by vapour deposition*. Nature **501** (2013) 395-398.
- [3] Q. Chen, H. Zhou, Z. Hong, S. Luo, H.-S. Duan, H.-H. Wang, Y. Liu, G. Li, and Y. Yang, *Planar heterojunction perovskite solar cells via vapor-assisted solution process*. J. Am. Chem. Soc. **136** (2013) 622-625.
- [4] T. Eisenbarth, T. Unold, R. Caballero, C.A. Kaufmann, and H.-W. Schock, *Interpretation of admittance, capacitance-voltage, and current-voltage signatures in Cu(In,Ga)Se₂ thin film solar cells*. J. Appl. Phys. **107** (2010) 034509.
- [5] J. Lauwaert, L. Van Puyvelde, J. Lauwaert, J.W. Thybaut, S. Khelifi, M. Burgelman, F. Pianezzi, A.N. Tiwari, and H. Vrielinck, *Assignment of capacitance spectroscopy signals of CIGS solar cells to effects of non-ohmic contacts*. Sol. Energ. Mat. Sol. Cells **112** (2013) 78-83.
- [6] A. Kubiaczyk, M. Nawrocka, and M. Igalszon, *Admittance measurements on CIGS solar cells*. Opto-Electron. Rev. **8** (2000) 378-381.
- [7] J.V. Li, S.W. Johnston, X. Li, D.S. Albin, T.A. Gessert, and D.H. Levi, *Discussion of some “trap signatures” observed by admittance spectroscopy in CdTe thin-film solar cells*. J. Appl. Phys. **108** (2010) 064501.
- [8] G. Friesen, E.D. Dunlop, and R. Wendt, *Investigation of CdTe solar cells via capacitance and impedance measurements*. Thin Solid Films **387** (2001) 239-242.
- [9] M. Burgelman, P. Nollet, and S. Degrave, *Modelling polycrystalline semiconductor solar cells*. Thin Solid Films **361–362** (2000) 527-532.
- [10] S.S. Hegedus and W.N. Shafarman, *Thin-film solar cells: device measurements and analysis*. Prog. Photovolt. Res. Appl. **12** (2004) 155-176.
- [11] H.-S. Kim and N.-G. Park, *Parameters Affecting I-V Hysteresis of CH₃NH₃PbI₃ Perovskite Solar Cells: Effects of Perovskite Crystal Size and Mesoporous TiO₂ Layer*. J. Phys. Chem. Lett. **5** (2014) 2927-2934.
- [12] H. Tian, L. Liu, B. Liu, S. Yuan, X. Wang, Y. Wang, T. Yu, and Z. Zou, *Influence of capacitance characteristic on dye-sensitized solar cell's IPCE measurement*. J. Phys. D Appl. Phys. **42** (2009)

- [13] I. Mora-Sero, G. Garcia-Belmonte, P.P. Boix, M.A. Vazquez, and J. Bisquert, *Impedance spectroscopy characterisation of highly efficient silicon solar cells under different light illumination intensities*. Energy Env. Sci. **2** (2009) 678-686.
- [14] G. Garcia-Belmonte, A. Munar, E.M. Barea, J. Bisquert, I. Ugarte, and R. Pacios, *Charge carrier mobility and lifetime of organic bulk heterojunctions analyzed by impedance spectroscopy*. Org. Electron. **9** (2008) 847-851.
- [15] J. Bisquert, G. Garcia-Belmonte, A. Munar, M. Sessolo, A. Soriano, and H.J. Bolink, *Band unpinning and photovoltaic model for P3HT:PCBM organic bulk heterojunctions under illumination*. Chem. Phys. Lett. **465** (2008) 57-62.
- [16] C. Zhao, X.F. Qiao, B.B. Chen, and B. Hu, *Thermal annealing effect on internal electrical polarization in organic solar cells*. Org. Electron. **14** (2013) 2192-2197.
- [17] B.B. Chen, X.F. Qiao, C.M. Liu, C. Zhao, H.C. Chen, K.H. Wei, and B. Hu, *Effects of bulk and interfacial charge accumulation on fill factor in organic solar cells*. Appl. Phys. Lett. **102** (2013) 193302.
- [18] C.F. Shih, K.T. Hung, H.J. Chen, C.Y. Hsiao, K.T. Huang, and S.H. Chen, *Incorporation of potassium at CuPc/C₆₀ interface for photovoltaic application*. Appl. Phys. Lett. **98** (2011) 113307.
- [19] L. Burtone, J. Fischer, K. Leo, and M. Riede, *Trap states in ZnPc:C₆₀ small-molecule organic solar cells*. Phys. Rev. B **87** (2013) 045432.
- [20] *Dye-sensitized Solar Cells*, K. Kalyanasundaram (Editor), EPFL Press (2010), pp. 526-529.